IEEE Access
Multidisciplinary ⋮ Rapid Review ⋮ Open Access Journal

Received February 1, 2021, accepted February 15, 2021, date of publication February 22, 2021, date of current version March 4, 2021.

Digital Object Identifier 10.1109/ACCESS.2021.3060794

Dynamic Curve Fitting and BP Neural Network With Feature Extraction for Mobile Specific Emitter Identification

QIN ZHANG[1], YU GUO[1], AND ZHENGYU SONG[2]
[1]School of Information and Electronics, Beijing Institute of Technology, Beijing 100081, China
[2]School of Electronic and Information Engineering, Beijing Jiaotong University, Beijing 100044, China

Corresponding author: Qin Zhang (zqbit@bit.edu.cn)

ABSTRACT As a critical technology in both civil and military fields, specific emitter identification (SEI) can identify signal sources according to their various features. Existing methods on SEI are mostly based on the prior knowledge of emitters, which are powerless in the non-cooperative scenario. In order to realize the unsupervised identification, the mobile SEI method based on fingerprint set construction and feedback classification algorithm is proposed in this paper. The proposed method first divides signal fingerprints into static features and dynamic features, where the former describe the inherent features of emitters, and the latter represent the moving state features of emitters. Then, the feedback classification algorithm composed of dynamic curve fitting and back propagation (BP) neural network is applied in the classification of signals. The dynamic curve accomplishes the first classification and the results with high credibility are used to train the BP neural network which accomplishes the final classification. Simulation results demonstrate that the proposed method can complete the identification of mobile specific emitter sources in the unsupervised state with more than 95% identification rate.

INDEX TERMS SEI, curve fitting, signal fingerprint, BP neural network.

I. INTRODUCTION

In recent years, specific emitter identification (SEI) has been recognized as a significant technology in both civil and military fields [1]. By classifying the received signals, the nature and threat levels of signals can be inferred, which plays an important role in the monitoring and identification of signals.

The SEI system mainly consists of two parts, i.e., the signal fingerprint set construction and classification. The signal fingerprint set construction refers to creating the unique feature set which can be employed to represent the received signals and associate with emitter individuals. Following the construction, SEI can be accomplished by sorting these fingerprints into different categories which represent different emitter individuals.

On one hand, with the advent of information technology revolution, various new multi-functional emitters have been applied, leading to more complex electromagnetic environments. Hence, the challenging problem arising in SEI is that traditional methods based on heuristic knowledge or a large number of training samples cannot be implemented. Under such circumstances, unsupervised identification method which does not need any prior knowledge is of great significance. On the other hand, with the continuously increasing demands for the identification, it is not only required to identify different types of emitter individuals with different modulation types or parameters, but also expected to accomplish the identification for the same type of emitters. The main SEI components are illustrated in Fig. 1.

In general, each emitter individual has unique circuit structure and electronic device. Thus, signals emitted by different individuals have different features even under the same modulation type and parameters [2]. According to the duration of time, the signal features can be divided into transient features and steady-state features. Transient features can always be extracted from the instantaneous amplitude, phase, and frequency of the received signals [3]. However, it is difficult in detecting the start and the end of transient signal precisely and satisfying the requirements of the sample rate transient analysis [4]. Thus, the steady-state features with long duration time

The associate editor coordinating the review of this manuscript and approving it for publication was Yue Zhang.

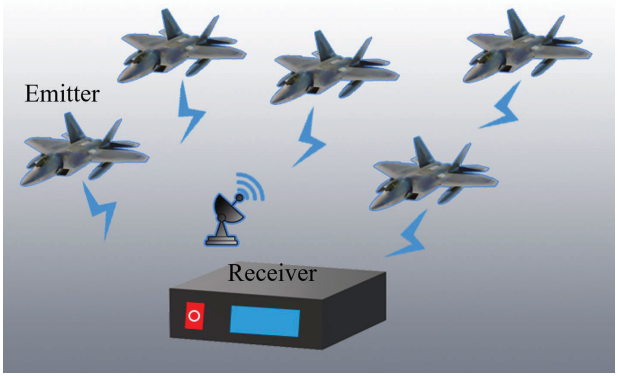

FIGURE 1. The main SEI components.

and stable performance are more conducive to processing and analysis, since they can be obtained from the time, frequency and transformed domains of the received signals.

In order to extract the steady-state features, Kawalec and Owczarek [5] propose the feature vector which combines signal feature parameters in the time and frequency domains. Sui *et al.* [1] perform wavelet transformation on the signal, where hierarchy and granularity are used to indicate the subtle feature information of signals emitted by different emitter individuals. The authors in [6] and [3] extract the energy entropy and color moments as identification features to cope with the SEI problems in both single-hop and relaying scenarios. The authors in [7] utilize power spectral density and adjacent channel power ratio (ACPR) as fingerprint features. Then, the principal component analysis (PCA) is employed to reduce the dimension of features. The above-mentioned features are utilizable due to they are not exactly the same for different emitter individuals. However, when the emitter individuals move in different states, it can also be considered to distinguish them by the moving state information.

The classification is mainly achieved by traditional and intelligent methods. The traditional methods require lower computational complexity, which are suitable for the scenarios with low-density emitters. For example, the authors in [8] and [9] employ feature matching and Dezert-Smarandache theory to accomplish the classification, respectively. In contrast with traditional methods, intelligent methods have higher identification accuracy for large volume of data and multi-feature identification. In [4],the authors employ support vector machine (SVM) to classify the fingerprint composed by overall and subtle transient features. In [10], SVM is used to accomplish the classification with the features extracted by empirical mode decomposition (EMD), but the classification performance of SVM depends on the selection of the kernel function. In [11], the neural network is employed with the feature vectors composed by signal parameters of the pulse repetition interval (PRI) and pulse width (PW), and it has strong learning ability and robustness. However, the ability for data mining is insufficient. After entering the era of deep learning, Xu *et al.* [12] bring forward the three-way incremental learning algorithm for emitter identification, which is adaptive to the increase of emitter types and samples. In [13], the method applying Convolutional Neural Networks (CNN) as feature learners and extractors is proposed. However, the methods in [12] and [13] both depend on the differences of the signal modulation types or modulation parameters. Thus, they are not applicable to the identification for the same type of emitters.

In summary, regarding the identification of emitter individuals which emit signals with the same parameters, the current research is based on the existing fingerprint database or other priori knowledge, which are only suitable for the cooperative or semi-cooperative targets. To overcome this difficulty, in this paper, we propose an unsupervised mobile SEI method, where no prior knowledge is required for the identification. The main contributions of this paper can be summarized as follows: (1) We propose an unsupervised SEI method for the scenario where there is no prior knowledge about the emitter individuals, and the types of emitters are all the same, i.e., there are no differences in signal modulation types or parameters. The proposed method consists of two parts, namely the signal feature extraction and the classification algorithm. (2) In the signal feature extraction, as an important supplement to the transient and steady-state features, the moving state features are explored as fingerprint for mobile SEI. With more kinds of features added to the signal feature set, the identification rate can be improved. (3) For the classification algorithm, we propose the feedback classification algorithm composed of dynamic curve fitting and back propagation (BP) neural network. Compared with the K-Means clustering algorithm, the proposed feedback classification algorithm can achieve more stable performance and higher identification rate.

The rest of this paper is organized as follows. First, the emitter signal model is given in Sec. II. Then, Sec. III introduces the data preprocessing and signal fingerprint construction. Next, Sec. IV presents the classification algorithm based on BP neural network and dynamic curve fitting. Finally, the simulation results and conclusions are discussed in Secs. V and VI, respectively.

II. SIGNAL MODEL

The SEI system diagram, as shown in Fig. 2, is composed of two parts, i.e., reconnaissance and identification. For the part of reconnaissance, signals received by radar are initially processed. Then, specific emitter signals studied in this paper are sorted out and stored. For the part of identification, it consists of the feature extraction module, fingerprint construction module, classification and result storage module. The part of identification aims at identifying the received signals from the emitter sources.

The signals studied in this paper are in the offset quadrature phase shift keying (OQPSK) format, and all of them have the same modulation parameters. Thus, the signal radiated from an ideal emitter can be modeled as

$$s_0(t) = I(t)\cos(\omega_0 t) - Q(t)\sin(\omega_0 t), \tag{1}$$

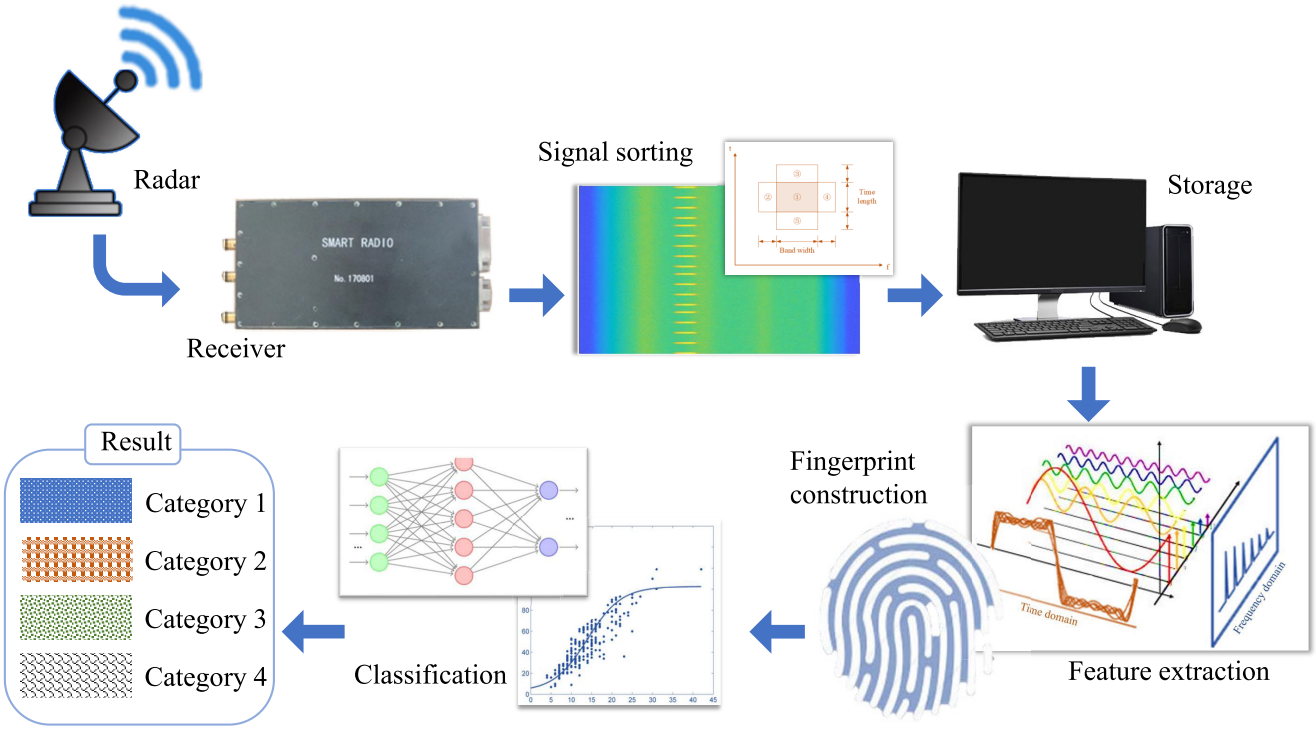

FIGURE 2. The SEI system diagram of the proposed method.

where ω_0 denotes the center carrier frequency of the received signal. $I(t)$ and $Q(t)$ represent the co-directional and quadrature branch signals of baseband, which can be expressed as

$$I(t) = \sum_n a_n g(t - nT_s), \tag{2}$$

$$Q(t) = \sum_n b_n g(t - nT_s - \frac{T_s}{2}), \tag{3}$$

where a_n and b_n represent the n-th signal symbol, and T_s represents the symbol period.

Taking the impacts of Doppler frequency and noise into consideration, the received signal can be expressed as

$$s(t) = I(t)\cos((\omega_0 + \Delta\omega)t) - Q(t)\sin((\omega_0 + \Delta\omega)t) + n(t), \tag{4}$$

where $\Delta\omega$ is the signal frequency offset, and $n(t)$ represents the noise.

III. FINGERPRINT SET CONSTRUCTION BASED ON PARAMETER EXTRACTION

A. DATA PREPROCESSING

In this section, the extraction of specific emitter signals will be completed, i.e., detecting and extracting target signals from noise, interference and other non-target signals, and then storing them for the identification.

Short-time Fourier transform (STFT) is employed to transform the signal into time-frequency domain. The definition of STFT is

$$STFT_s(t, f) = \int_{-\infty}^{\infty} [s(t')w^*(t' - t)]e^{-j2\pi ft'}\, dt, \tag{5}$$

where $w^*(t' - t)$ is the window function, which determines the resolution of the signal in the time-frequency domain.

In order to reduce the impact of noise, the STFT results of multiple windows are accumulated, which can be expressed as

$$STFT_s(t_k, f) = \sum_{n \in N_{acc} * [k, k+1)} STFT_s(t_n, f), \tag{6}$$

where N_{acc} is the cumulative number of windows.

After the above processing on the received signal, the cumulative result of STFT is obtained and shown in Fig. 3. The color represents signal strength. The horizontal and vertical axis are the relative frequency and time values, respectively. The actual frequency and time can be calculated by

$$F_{real} = F_{relative} * F_s / N_{fft}, \tag{7}$$

$$T_{real} = T_{relative} * N_{acc} / F_s, \tag{8}$$

where F_s is the sampling rate of received signal, and N_{fft} is the number of FFT points.

Next, the signal extraction can be achieved by the template matching method [14], and then the target signal is stored for the following processing.

Following the data preprocessing, the signal fingerprint extraction is accomplished. In order to extract the steady-state

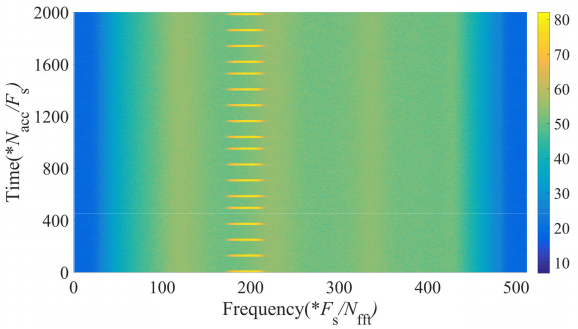

FIGURE 3. The cumulative result of STFT.

features in the time, frequency and transformed domains, parameter estimation will be completed during the signal receiving and demodulating. In the parameters, there are emitter individual inherent features and moving state features. These parameters will be employed to construct the signal fingerprint.

The inherent features of the emitter individuals stem from the unintentional modulation on pulse (UMOP), including the features of noise, frequency source and spurious, etc. The moving state features of emitter individuals are from the differences of transmission paths. When emitter individuals are in different moving states, the Doppler frequencies for the received signals are different.

All above, the signal fingerprint can be constructed by the parameters including Doppler frequency, SNR and pulse parameters, etc. In the following, we will introduce the parameter estimation in detail.

B. DOPPLER FREQUENCY ESTIMATION

Doppler effect is caused by the relative motion between the emitter and receiver. The Doppler frequency can be expressed as

$$\Delta f = (v\cos\theta)/\lambda, \tag{9}$$

where v is the speed of emitter. θ is the angle between the movement direction of emitter and signal emission, and λ is the signal wavelength.

It can be seen from (9) that Doppler frequency will change with the variation of emitter's speed or the relative position between emitter and receiver, especially for the signal with short wavelength. Besides, Doppler spread measures the coherence time, related to the rate of change, of wireless communication channels [15]. The change of moving state and channel characteristics have significant effects on Doppler frequency, which provides an opportunity to apply Doppler frequency to distinguish emitter individuals.

By transforming the received signal shown in (4) to the baseband, the quadrature and parallel components can be found as

$$\begin{aligned} s_{imid}(t) &= (I(t)\cos((\omega_0+\Delta\omega)t) \\ &\quad -Q(t)\sin((\omega_0+\Delta\omega)t))\cos(\omega_0 t) \\ &= I(t)(\cos((2\omega_0+\Delta\omega)t)+\cos(\Delta\omega t)) \\ &\quad -Q(t)(\sin((2\omega_0+\Delta\omega)t)+\sin(\Delta\omega t))+C_1, \end{aligned} \tag{10}$$

$$\begin{aligned} s_{qmid}(t) &= (I(t)\cos((\omega_0+\Delta\omega)t) \\ &\quad -Q(t)\sin((\omega_0+\Delta\omega)t))\sin(\omega_0 t) \\ &= I(t)(\sin((2\omega_0+\Delta\omega)t)-\sin(\Delta\omega t)) \\ &\quad -Q(t)(\cos((2\omega_0+\Delta\omega)t)-\cos(\Delta\omega t))+C_2, \end{aligned} \tag{11}$$

where C_1 and C_2 are the constants generated by the calculation of the signal phase. The baseband signal $s_b(t)$ can be obtained by processing s_{imid} and s_{qmid} with the low-pass filter, which can be expressed as

$$\begin{aligned} s_b(t) &= s_{bI}(t)+s_{bQ}(t) \\ &= LP(s_{imid}(t))+LP(s_{qmid}(t)) \\ &= I(t)(\cos(\Delta\omega t)-j\sin(\Delta\omega t)) \\ &\quad +Q(t)(\cos(\Delta\omega t)+j\sin(\Delta\omega t)) \\ &= I(t)\exp(-j\Delta\omega t)+jQ(t)\exp(j\Delta\omega t), \end{aligned} \tag{12}$$

where $LP(\bullet)$ represents the signal processed with the low-pass filter.

Then, by calculating the square spectrum of $s_b(t)$, we have

$$\begin{aligned} s_b^2(t) &= I^2(t)\exp(-j2\Delta\omega t) \\ &\quad - Q^2(t)\exp(j2\Delta\omega t)+2jI(t)Q(t) \\ &= I^2(t)\exp(-j2\Delta\omega t)-Q^2(t)\exp(j2\Delta\omega t), \end{aligned} \tag{13}$$

$$\begin{aligned} \mathscr{F}\{s_b^2(t)\} &= \mathscr{F}\{I^2(t)\}*\delta(\omega+2\Delta\omega) \\ &\quad -\mathscr{F}\{Q^2(t)\}*\delta(\omega-2\Delta\omega), \end{aligned} \tag{14}$$

where $\mathscr{F}(\bullet)$ represents the signal processed with FFT. Suppose the spectrum of $I^2(t)$ is $P(f)$. Combining (2) and (3), the following expressions can be obtained as

$$\mathscr{F}\{I^2(t)\} = \mathscr{F}\{\sum_n a_n^2\, g^2(t-nT_s)\} = P(f), \tag{15}$$

$$\begin{aligned} \mathscr{F}\{Q^2(t)\} &= \mathscr{F}\{\sum_n a_n^2\, g^2(t-nT_s-\frac{T_s}{2})\} \\ &= P(f)e^{-j\pi fT_s}, \end{aligned} \tag{16}$$

$$\mathscr{F}\{s_b^2(t)\} = P(f+2\Delta f)-P(f-2\Delta f)e^{-j\pi(f-2\Delta f)T_s}, \tag{17}$$

where $\Delta f = \frac{\Delta\omega}{2\pi}$. Obviously, $\mathscr{F}\{s_b^2(t)\}$ achieve the maximum when $f = 2\Delta f \pm \frac{1}{T_s}$, which are the two peak positions of $\mathscr{F}\{s_b^2(t)\}$. The frequencies of the two peak positions can be calculated by

$$f_1 = 2\Delta f + \frac{1}{T_s}, \tag{18}$$

$$f_2 = 2\Delta f - \frac{1}{T_s}. \tag{19}$$

Then, the Doppler frequency parameter Δf can be obtained by

$$\Delta f = \frac{(f_1+f_2)}{4}. \tag{20}$$

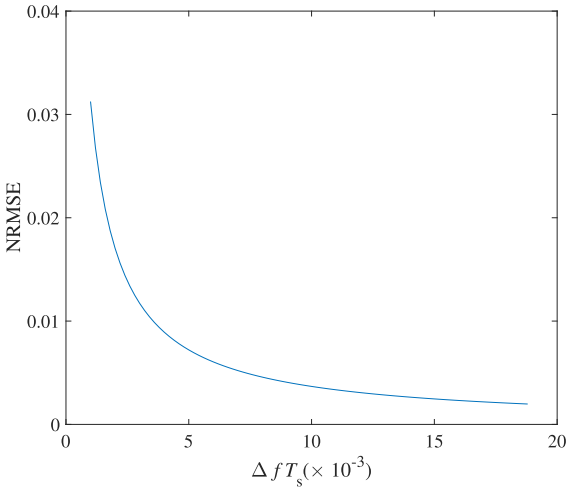

FIGURE 4. The NRMSE *vs.* ΔfT_s for the proposed doppler frequency estimation method.

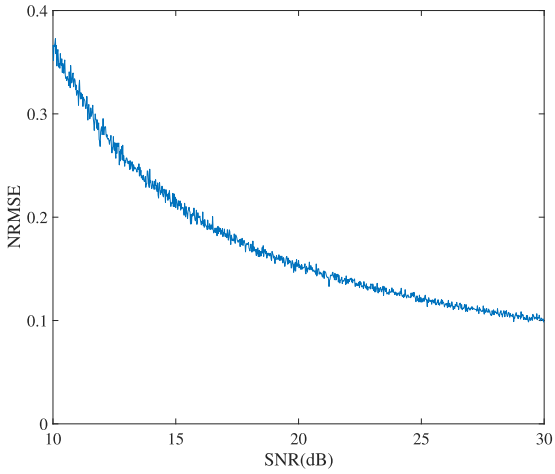

FIGURE 5. The NRMSE *vs.* SNR for the proposed SNR estimation method.

In order to measure the performance of the proposed Doppler frequency estimation method, it is necessary to calculate the normalized root-mean-square error (NRMSE) of Doppler frequency [16], which can be expressed as

$$\epsilon_{NR\Delta f} = \frac{[(\Delta f - f_d)^2]^{1/2}}{f_d}, \tag{21}$$

where f_d is the actual value of Doppler frequency. The NRMSE versus ΔfT_s for the proposed Doppler frequency estimation method is demonstrated in Fig. 4. According to the performance in [15], the estimation in this paper is reliable, and thus it can be applied to construct the signal fingerprint.

At the same time, in order to perform curve fitting on the Doppler frequency, we also denote the reception time of each received signal as a feature.

C. SNR ESTIMATION

There are two main reasons for the differences in SNR of different emitter individuals. On one hand, from the statistical point of view, there are slight differences on the noise features of specific emitters due to the distinction in internal devices; On the other hand, the distinction in transmission paths, including different shadow fading, multipath fading, and free space loss, also causes huge differences in signal attenuation. Hence, the SNR of received signals involves both the information of transmission paths and the individual features of emitters. The M2M4 algorithm proposed in [17] can be used to estimate the SNR of the received signals.

Next, we calculate the NRMSE of SNR to measure the performance of the proposed SNR estimation method. The NRMSE of SNR can be expressed as

$$\epsilon_{NRS} = \frac{[(S_{cal} - S)^2]^{1/2}}{S}, \tag{22}$$

where S is the actual value of SNR and S_{cal} is the estimated value of SNR. The NRMSE versus S for the proposed SNR estimation method is displayed in Fig. 5. According to the performance of the approach proposed in [18], the estimation is reliable, and thus it can be used to construct the signal fingerprint.

D. ENVELOPE DROP ESTIMATION

The signals emitted by different emitter individuals have different envelope features. Firstly, the signal envelope contains rich nonlinear features, because of the different parasitic modulations caused by phase noise and spurious output. Secondly, the transmission clutter and multipath effects can also cause dramatic changes in pulse envelope [19]. Thus, the envelope features of received signals can be used as fingerprint to identify different emitter individuals.

By combining (10) to (12), the received signal envelope can be obtained from the parallel and quadrature components of the signal, which can be expressed as

$$u(l) = \sqrt{s_{bI}^2(l) + s_{bQ}^2(l)}. \tag{23}$$

The schematic diagram of the pulse envelope is shown in Fig. 6, where the pulse envelope features can be extracted mainly from the rising edge, top and falling edge of the envelope. Two parameters of signal envelope, ascending time and envelope drop [20], are selected to construct the signal fingerprint set.

The time required for pulse envelope to rise from 10% to 90% of the average pulse top value is defined as the signal pulse envelope ascending time, and the envelope drop can be obtained by

$$\overline{u_t} = \frac{1}{N}\sum_{l=1}^{L} u_t(l), \tag{24}$$

$$V = \frac{1}{N}\sum_{l=1}^{L}(u_t(l) - \overline{u_t})^2, \tag{25}$$

where $u_t(l)$ is the sequence of $u(l)$ in the top of the signal pulse envelope.

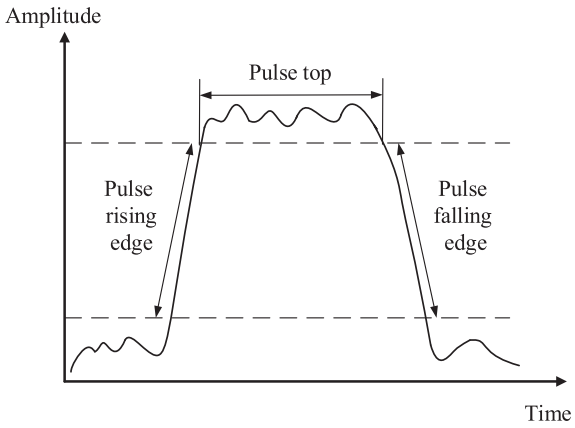

FIGURE 6. The schematic diagram of the pulse envelope.

E. SIGNAL FINGERPRINT CONSTRUCTION

In order to better apply the classification algorithm, the signal fingerprint is built in the form of matrix $\mathbf{D}(\mathbf{D} \in \mathbf{R}_{M\times R})$, where M is the number of received signals and R is the number of parameter types. d_{mr} represents the r-th fingerprint feature of the m-th received signal.

IV. IDENTIFICATION METHOD BASED ON FEEDBACK CLASSIFICATION ALGORITHM

In this section, based on the signal fingerprint constructed in the previous section, the feedback classification algorithm is presented which combines the curve fitting and BP neural network to achieve better identification performance. Traditional K-Means clustering algorithm is also introduced briefly in order to conduct performance comparisons.

A. CURVE FITTING

Curve fitting refers to applying a continuous curve to approximate the functional relationship between the coordinates represented by discrete point groups on the plane. Considering there are $N+1$ known points (x_i, y_i), $i = 0, 1, 2, \ldots, n$, where $x_i \neq x_j$ (for $i \neq j$), curve fitting is to seek function $y(x)$ which is the closest to all data points [21]. It is specifically called polynomial fitting when the selected $y(x)$ has the form as

$$y(x) = a_0 + a_1x + a_2x^2 + \ldots + a_mx^m. \tag{26}$$

Curve fitting is suitable for the classification of dynamical parameters, which is Doppler frequency in this paper. In order to reduce the computational complexity, the relative reception time, which means the differential sequence of fingerprint reception time, is employed to complete the curve fitting. The classification results can be obtained by fitting $(t_i, f_i)(i \in [1, M])$ into different curves.

The emitter is generally carried by a fighter whose trajectory includes straight-line flight and turning flight [22]. In order to simplify its moving state, we can observe the trajectory in a short time where the trajectory can be approximated as a straight line and the relative position of the emitter and receiver remains unchanged. In this cases, the Doppler frequency is determined by the speed only. Then, the partial fitting method using quadratic polynomials and least squares can be applied to fit the Doppler frequency in each short period of time.

If we have accomplished the classification of $m-1$ fingerprints, and they have been classified into several categories, the classification category for the m-th fingerprint should be determined. When all the fingerprints are classified, the curve fitting classification results can be obtained.

When determining whether the m-th fingerprint (t_m, f_m) should be classified into the e-th category, $(t_i, f_i)(i \in (\max(1, i-15), m))$ of the last 15 fingerprints in the e-th category are chosen for curve fitting (if there are less than 15 fingerprints, taking all fingerprints in the e-th category). Suppose the fitting result is $h_e(t)$. In order to evaluate the performance of the fitting curve $h_e(t)$, the error between the actual value y_i and the predicted value $h_e(x_i)$ of each sample point needs to be measured. The fitting objective is to minimize the sum of errors. The most commonly used method of curve fitting error calculation is the least squares method, whose basic idea is to seek $\{a_0, a_1, \ldots, a_m\} = \arg\min(\epsilon)$, where ϵ can be expressed as

$$\epsilon = \sum_{i=0}^{n}(y(x_i) - y_i)^2. \tag{27}$$

Since there are several curves that the current point can be added to, it is necessary to determine the most reasonable curve. On one hand, considering the fitting error, the current fingerprint is supposed to be added to the curve which will have the minimal internal error after the current point is added, where the internal error $\epsilon_{in}(e)$ can be expressed as

$$\begin{aligned}\epsilon_{in}(e) &= \sum_{i=0}^{m}(h_e(t_i) - f_i)^2, \\ i &= \max(1, i-15), \ldots, m-1, m.\end{aligned} \tag{28}$$

On the other hand, it is necessary to determine whether there are suitable curves to join the 15 fingerprints after the current one. The current fingerprint is supposed to be added to minimize the external error $\epsilon_{ex}(e)$, which can be expressed as

$$\begin{aligned}\epsilon_{ex}(e) &= \sum_{k}\min(h_k(t_j) - f_j), \\ &j = 1, 2, \ldots, n;\ k = m+1, m+2, \ldots, \min(m+15, M).\end{aligned} \tag{29}$$

In order to determine which category is the most suitable for the current fingerprint to add to, the empty set $\mathbf{U}$ is initialed. Firstly, by comparing $(\epsilon_{in}(e), \epsilon_{ex}(e))(e \in (1, n))$ with the external error threshold and internal error threshold, we can record the categories whose errors are greater than the thresholds and add their serial numbers to $\mathbf{U}$. Secondly, by calculating the change of Doppler frequencies in each category, we can record the categories where the values are greater than the mutation threshold. Then, their serial numbers are added to the set $\mathbf{U}$. Finally, expect for the categories

Algorithm 1 The curve fitting classification algorithm

1. Initialize the fingerprint feature matrix $\mathbf{D}_{M\times R}$. Let the current number of category be $N = 0$. Denote the serial number of category where the current fringerprint will be added as $n = 0$, and the current serial number of fingerprint as $m = 1$;
2. Calculate the relative reception time of every fingerprint;
3. **while** $m<M$ **do**
4. Select the relative reception time and Doppler frequency of the m-th fingerprint (t_m, f_m) for curve fitting.
5. **while** $n<N$ **do**
6. Calculate $(\epsilon_{in}(n), \epsilon_{ex}(n))$ and the change of Doppler frequency after adding (t_m, f_m) to the n-th category. Then, $n \leftarrow n + 1$.
7. **end while**
8. If there are categories meeting the fitting error thresholds, select the category with the smallest fitting error for the fingerprint to join in. Otherwise, create a new category and let it be the first fingerprint of the category, $N \leftarrow N+1$. Then, $m \leftarrow m+1$;
9. **end while**
10. Considering the fingerprints on the same curve are emitted by the same emitter, label the fingerprints in $\mathbf{D}_{M\times R}$ and obtain the classification result matrix $\mathbf{E}$.

whose serial numbers recorded in $\mathbf{U}$, the current fingerprint will be added to the category which has the smallest internal error. If there is no remained category ($\mathbf{U} = [1, n]$), the fingerprint isn't recorded in any of the current categories. In this case, a new category is created and the current fingerprint is the first one in the new category.

The curve fitting classification algorithm can be summarized in **Algorithm 1**.

B. NEURAL NETWORK

BP neural network, composed of input layer, output layer and hidden layer, is the feedforward network trained by error back propagation algorithm. It has an outstanding advantage in flexible network structure and strong nonlinear mapping ability. The number of network's intermediate layers and neurons in each layer can be arbitrarily set according to specific circumstances [23].

The classification problem is, essentially, to complete the mapping from the fingerprint space to the decision space, and the three-layer BP neural network can complete any n-dimensional to m-dimensional mapping. Therefore, the BP neural network can be used to solve the classification problem.

The dimensions of BP neural network's input layers are determined by the signal fingerprint feature set $\mathbf{D}_{M\times R}$. According to the actual requirements, it equals to the number of fingerprint features except Doppler frequency and reception time.

Algorithm 2 The selection algorithm of highly reliable fingerprints

1. Obtain the classification result matrix $\mathbf{E}$ by Algorithm 1;
2. Set a time window with appropriate length. Then, calculate the average Doppler frequency of different categories in the time window;
3. Calculate the differences between the average Doppler frequencies of every two categories. If there is a value below the threshold, denote the time window as an uncertain window, and record the serial number of the uncertain category in this window. Otherwise, denote it as a certain window;
4. Find the longest continuously certain window, and put the fingerprints in the continuous window into the deterministic fingerprint set $\mathbf{E}_c$, while the other fingerprints are put into the uncertain fingerprint set $\mathbf{E}_u$;
5. Denote the fingerprint set $\mathbf{E}_c$ as the training set and $\mathbf{E}_u$ as the test set.

The dimensions of BP neural network's output layers are determined by the result of curve fitting classification. If assuming the curve fitting classification divides the signal fingerprint into Z categories, the number of output layers is Z.

As for the selection of the number of hidden nodes, a large number of nodes leads to longer learning time. On the contrary, a few number of nodes results in poor fault tolerance of the network. Hence, according to the empirical formula proposed by [23], the number of nodes can be calculated by

$$N_h = (N_{in} + N_{out})/2, \tag{30}$$

where N_{in} represents the number of input layers and N_{out} is the number of output layers.

For the BP neural network in this paper, it has three input nodes, three hidden nodes and four output nodes. According to the training parameters of the BP neural network in [24], the learning rate in this paper is $\eta = 0.001$, and the momentum constant is $\alpha = 0.9$. For the maximum training times, it is set as $e = 1000$ and the training accuracy is $g = 0.01$.

The highly reliable fingerprints in the curve fitting results are selected as the training set of the BP neural network. And the selection algorithm for the highly reliable fingerprints is summarized in **Algorithm 2**.

Following the initialization of the neural network, the static fingerprint features, which are recorded in the training set, can be used to train the network. Afterwards, the probability that each fingerprint in test set belongs to a specific category can be obtained by the neural network.

C. FEEDBACK ALGORITHM DESIGN

The flow chart of the feedback classification algorithm is shown in Fig. 7. The key idea of the algorithm is as follows. Firstly, the first classification with curve fitting classification

Algorithm 3 Feedback classification algorithm

1. Complete the first classification by curve fitting with the dynamic features in $\mathbf{D}_{M\times R}$, and obtain the classification result matrix $\mathbf{E}$;
2. By Algorithm 2, select the fingerprints with high reliability to construct the training set $\mathbf{E}_c$ for BP neural network, and the other fingerprints as test set $\mathbf{E}_u$;
3. Initialize the neural network, and train the network with static features in $\mathbf{E}_c$. Obtain the probability that each fingerprint in $\mathbf{E}_u$ belongs to a specific category;
4. Obtain the final classification result matrix according to the probabilities.

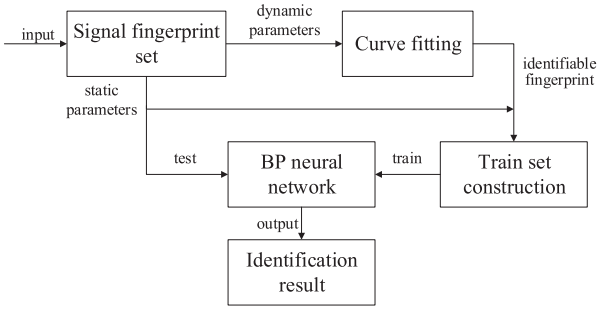

FIGURE 7. The flow chart of feedback classification algorithm.

algorithm is used to obtain the preliminary results. Secondly, the signal fingerprints with higher reliability are selected as the training set of neural network. Thirdly, the signal fingerprints are input into the trained network in order to obtain final identification results. The feedback classification algorithm is summarized in **Algorithm 3**.

D. THE IMPROVED K-MEANS CLASSIFICATION ALGORITHM

K-Means algorithm is an unsupervised cluster algorithm, where the distance is used as an indicator to measure the similarity of samples. The key idea of K-Means algorithm is to divide n data objects into K clusters, aiming at reducing the sum of distance between each data point in each cluster to the center of the cluster. In this way, the sample points in the same cluster are more similar than the samples among different clusters. Hence, in order to improve the applicability of K-Means classification algorithm, a criterion is necessary to determine the reasonable number of categories automatically.

After $\mathbf{D}_{M\times R}$ is divided into N categories, we can obtain the variances of different fingerprint parameters in different categories. Then, the average variances of different categories for the same parameter can be calculated by

$$V_r(N) = \frac{1}{N}\sum_n (V_{rn}), \tag{31}$$

where V_{rn} is the variance of the r-th fingerprint in the n-th category. As the number of categories N increases,

Algorithm 4 Improved K-Means classification algorithm

1. Initialize the fingerprint feature matrix $\mathbf{D}_{M\times R}$. Denote the number of category as $N = 1$;
2. Divide M fingerprints into N categories with K-Means algorithm;
3. Calculate the average variance $V_r(N)$ of different fingerprint parameters in different categories;
4. If $N \geq 2$, calculate the changing rate of $V_r(N)$. If the changing rate is below the threshold, mark the corresponding fingerprint;
5. If all the fingerprints have been marked, continue Step 6. Otherwise, $N \leftarrow N + 1$, and go to Step 1;
6. Denote the number of categories corresponding to the minimum V_r of r-th fingerprint as $N_{min}(r)$.
7. Find the modes of N_{min}. If there is only one mode, take it as the number of categories. Otherwise, take the mode corresponding to the smallest sum variance as the number of categories.
8. Obtain the number of categories and the classification result matrix.

$V_r(N)(r \in [1, R])$ will become smaller. When $V_r(N)$ remains almost unchanged, it is believed that the classification performance is the best, and the corresponding N is the most reasonable number of categories.

In summary, the improved K-Means classification algorithm can be summarized as **Algorithm 4**.

E. COMPUTATIONAL COMPLEXITY

In the following, we analyze the computational complexity of the proposed feedback classification algorithm.

(1) Assume the number of sampling points for each fingerprint is N_s and the order of the low pass filter is N_f. The Doppler frequency estimation is analyzed from (9) to (20), where we can infer that the computational complexity is $\mathcal{O}(M(N_s + N_f)^2)$.

(2) The computational complexity of the SNR estimation method in [17] is $\mathcal{O}(MN_s)$.

(3) The envelope drop estimation is analyzed from (23) to (25), and the computational complexity is $\mathcal{O}(M(N_s + L))$.

(4) Assuming the numbers of calculated category and the point for curve fitting are a and P, respectively, then the computational complexity of the proposed feedback classification algorithm and the improved K-Means classification algorithm are $\mathcal{O}(M(aP + R))$ and $\mathcal{O}(aMR)$, respectively.

The complexity of the overall identification process is $\mathcal{O}(M((N_s+N_f)^2+L+aP+R))$. Compared with the clustering algorithm proposed in [4], the computational complexity of the proposed algorithm is relatively lower.

Regarding the trade-off between the complexity and performance, we find that the number of fingerprints determines the computational complexity directly. A large number of fingerprints leads to complicated calculation, while a few of fingerprints affects the identification rate. Besides, a suitable

TABLE 1. The parameters of experimental environments.

Environment No.	Emitter No.	$d_0(\times 10^3\mathrm{m})$	$d_1(\times 10^3\mathrm{m})$	$a(\mathrm{m/s^2})$	$v_0(\mathrm{m/s})$	$v_1(\mathrm{m/s})$	$r(\mathrm{dB})$
1	1	25	15	0	100	100	40
	2	25	15	7	30	200	40
	3	12.8	8	3	150	200	20
	4	12.8	8	1	80	150	55
2	1	25	15	0	100	100	50
	2	25	15	7	30	200	50
	3	12.8	8	3	150	200	10
	4	12.8	8	1	80	150	45
3	1	25	15	3	10	80	40
	2	25	15	0	50	60	40
	3	12.8	8	2	50	80	20
	4	12.8	8	2	10	60	55

d_0 represents the distance between the emitter individuals and the receiver; d_1 represents the distance from the receiver to the moving direction of the emitter individuals; a is the acceleration of the emitter individuals; v_0 and v_1 represent the initial and maximum speeds of the emitter individuals; r is the attenuation amplitude of the emitter individuals.

number of partial curve fitting points is of great importance. This is because if the number of partial curve fitting points is larger, the calculation will be more complicated, but the fitting error of the moving state is smaller. On the contrary, if the number of partial curve fitting points is smaller, the computational complexity will be lower and the fitting error of the moving state is lager.

V. SIMULATION RESULTS

In this section, we evaluate the performances of the proposed algorithms. In the simulations, four specific emitter sources emit OQPSK signals with the same modulation parameters, and the signals are captured by an antenna which is connected to a digital receiver. The signal parameters are extracted to make up the fingerprint set. Then, the fingerprint construction results of the received signal and identification results are illustrated. Finally, the identification rate and accuracy rate of the feedback classification algorithm and K-Means algorithm are presented and compared.

A. SIMULATION CONDITIONS

In terms of the channel conditions, the experiment and simulations are performed based on the air-to-ground channels. The channel parameters are functions of the elevation angle, which depends on both the emitter altitude in the air and the horizontal (or 2-D) distance with the corresponding ground receiver [25]. Meanwhile, all the four emitter individuals are set in different positions. For the emitter individuals. we employ four signal sources of the same model to emit signals with the same parameters. The modulation format of the emitted signal is OQPSK. The carrier frequency and the symbol rate are set to 450MHz and 2.5MHz, respectively. By calculating the Doppler frequency in different cases, the real-time frequency offset is used to help the identification of the specific emitter. The parameters of the three experimental environments are shown in the Table 1.

B. PERFORMANCE METRICS

Assume the calculated number of categories is a, and the calculated classification result is $\mathbf{C}_i (i \in [1, a])$. The actual number of categories is b, and the actual classification result is $\mathbf{B}_j (j \in [1, b])$. Besides, suppose the category correspondence operation between $\mathbf{B}$ and $\mathbf{C}$ has been completed, where $\mathbf{C}_i$ has the highest similarity with $\mathbf{B}_{M(i)}$, and $\mathbf{B}_j$ has the highest similarity with $\mathbf{C}_{N(j)}$.

We propose two metrics to measure the classification performance of different algorithms, namely identification rate and accuracy rate, which are defined as

$$R_{id}(j) = \frac{Num(\mathbf{C}_{N(j)} \cap \mathbf{B}_j)}{\mathbf{B}_j}, \tag{32}$$

$$R_{ac}(j) = \frac{Num(\mathbf{B}_{M(i)} \cap \mathbf{C}_i)}{\mathbf{C}_i}. \tag{33}$$

It is expected that the difference between a and b is as small as possible. The more values of R_{id} are greater than the effective threshold, the more effective categories are identified. When R_{ac} is larger, the differentiating performance along different categories is better. For the global accuracy rate, it can be calculated by

$$R = \frac{Num(\bigcup_j \mathbf{C}_{N(j)} \cap \mathbf{B}_j)}{Num(\bigcup_j \mathbf{B}_j)}. \tag{34}$$

C. FINGERPRINT CONSTRUCTION RESULT

In this subsection, the results of signal fingerprint construction are shown by taking environment 1 as an example. The Doppler frequency extraction results are shown in Fig. 8. It can be observed intuitively that all Doppler frequency points can be connected in series by four curves. On each curve, the Doppler frequency is dynamically and continuously changing. There is no mutation in a short time, which meets the requirements of the curve fitting algorithm.

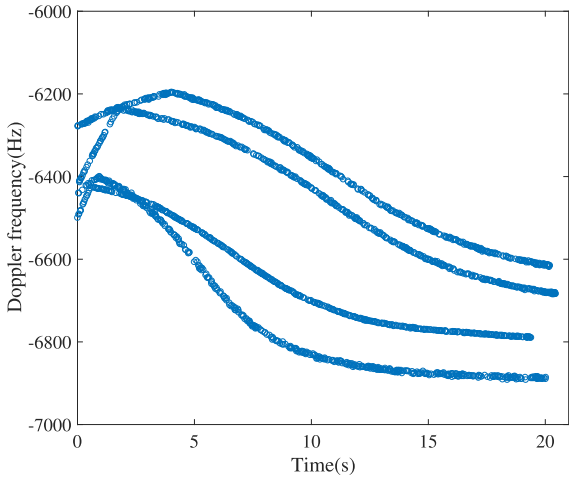

FIGURE 8. The extraction results of doppler frequency.

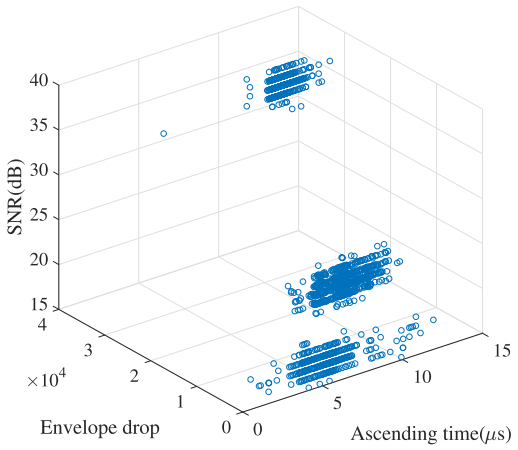

FIGURE 9. The static feature extraction result.

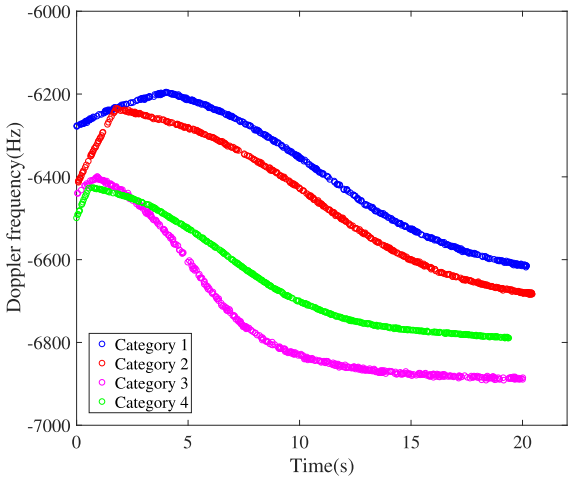

FIGURE 10. The ideal result of curve fitting algorithm for environment 1.

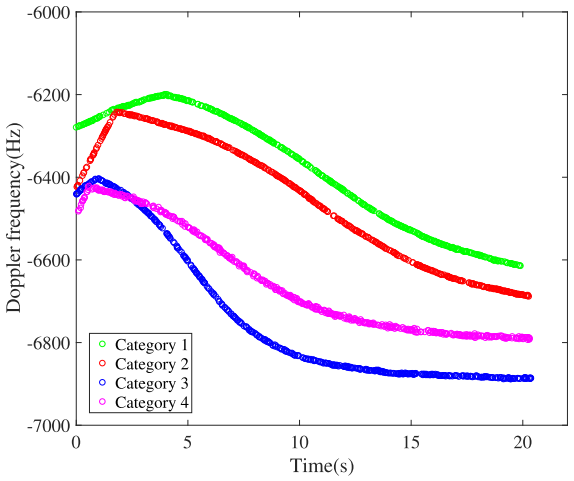

FIGURE 11. The ideal result of curve fitting algorithm for environment 2.

The extraction results of other fingerprint features are shown in Fig. 9. It can be seen that the points which represent static parameters are roughly divided into three categories. The points in each category are relatively concentrated without large-scale mutation, which provides us with the conditions of applying feedback classification algorithm and K-Means clustering algorithm for the classification.

D. IDENTIFICATION RESULT

1) CURVE FITTING CLASSIFICATION RESULTS

According to the simulation setting, the ideal results of curve fitting algorithm in the three environments are shown in Figs. 10-12. The four colors in the figures represent the signals of the four emitter sources.

The practical results of curve fitting algorithm (i.e., **Algorithm 1**) in the three environments are displayed in Figs. 13-15. The identification and accuracy rates of various emitter individuals are shown in Table 2. It can be observed from Figs. 13-15 that curve fitting algorithm basically completes the classification of specific emitter source signals. The identification performance is better when the Doppler frequencies are far away from each other. On the contrary, there will be misclassification where the Doppler frequencies are closer to each other, i.e., different curves may be incorrectly connected. By comparing the green curve in Fig. 13 and the curves in Fig. 10, it can be seen that the left and right sides, separated by the intersection of the green curve and the red curve, actually belong to different curves. Besides, it can be observed from Figs. 11 and 14 that there are also misclassification points in the areas where the red and purple points are close. To solve these problems, neural network classification is introduced on the basis of curve fitting classification.

2) FEEDBACK CLASSIFICATION RESULTS

In order to overcome the limitations of curve fitting, the neural network with static parameters is carried out in the simulations. The identification results of feedback classification algorithm (i.e., **Algorithm 3**) in the three environments are demonstrated in Figs. 16-18, where different colors represent different categories. The identification and accuracy rates

TABLE 2. Identification performances of the curve fitting algorithm.

Environment No.	Identification Performances	Individual Source ID			
		1	2	3	4
1	Identification rate (%)	91.75	89.31	90.19	95.24
	Accuracy rate (%)	94.93	91.23	89.67	88.89
	Global accuracy rate (%)	91.49			
2	Identification rate (%)	100.00	92.38	100.00	91.00
	Accuracy rate (%)	100.00	100.00	91.14	92.26
	Global accuracy rate (%)	95.83			
3	Identification rate (%)	85.96	81.68	99.81	99.61
	Accuracy rate (%)	100.00	99.61	85.34	83.05
	Global accuracy rate (%)	92.08			

TABLE 3. Identification performances of the feedback classification algorithm.

Environment No.	Identification Performances	Individual Source ID			
		1	2	3	4
1	Identification rate (%)	99.80	99.80	100.00	100.00
	Accuracy rate (%)	99.22	99.42	100.00	99.61
	Global accuracy rate (%)	99.90			
2	Identification rate (%)	100.00	94.06	100.00	98.82
	Accuracy rate (%)	100.00	100.00	94.38	98.75
	Global accuracy rate (%)	98.23			
3	Identification rate (%)	99.81	99.22	99.42	99.61
	Accuracy rate (%)	100.00	100.00	99.61	99.80
	Global accuracy rate (%)	99.85			

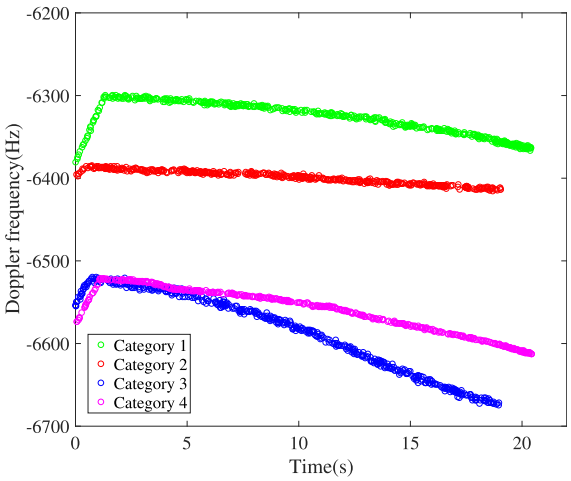

FIGURE 12. The ideal result of curve fitting algorithm for environment 3.

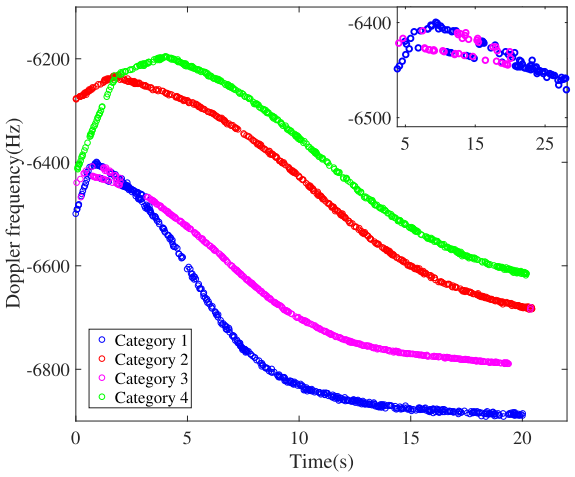

FIGURE 13. The practical result of curve fitting algorithm for environment 1.

of feedback classification algorithm are given in Table 3. It can be found that by the secondary classification, the global accuracy rates can achieve 99.9%, 98.23% and 99.85% in the three environments, while they are 91.49%, 95.83% and 92.08%, respectively, in Table 2, and the identification rate in each category is also improved. This is because the neural network makes full use of the information contained in static features to further distinguish different emitter individuals.

3) THE IMPROVED K-MEANS CLASSIFICATION RESULTS

In our simulations, samples are generally divided into 4 or 5 categories. For environment 1, the results when $K = 5$ and $K = 4$ are shown in Figs. 19 and 20, respectively. The corresponding identification and accuracy rates of the improved K-Means algorithm are shown in Tables 4 and 5.

Observing the results in Tables 4 and 5, we can see that when the value of K calculated by the improved K-Means algorithm is greater than the actual number of classes,

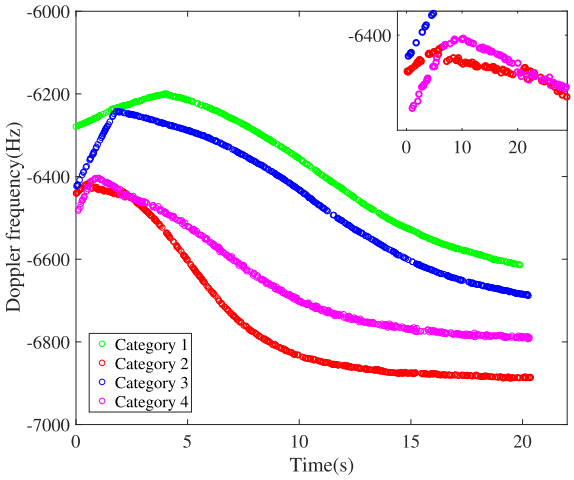

FIGURE 14. The practical result of curve fitting algorithm for environment 2.

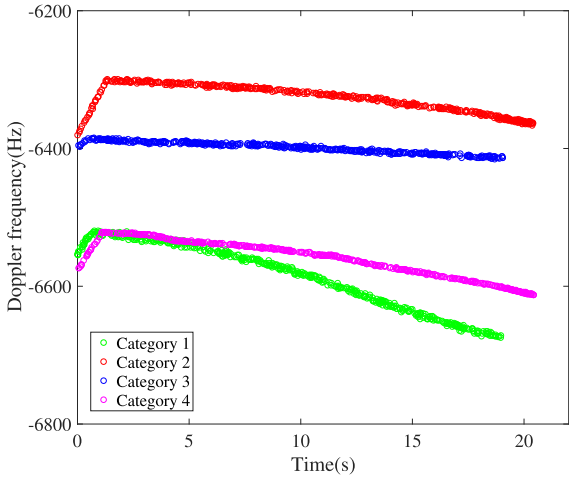

FIGURE 15. The practical result of curve fitting algorithm for environment 3.

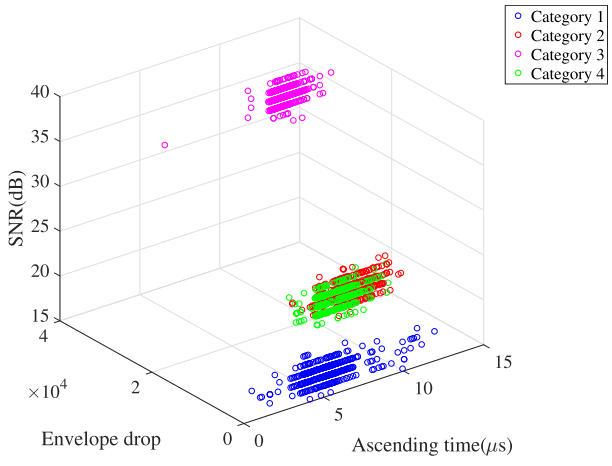

FIGURE 16. The identification result of feedback classification algorithm for environment 1.

a certain category is wrongly divided into two categories. Meanwhile, the identification rates are basically consistent

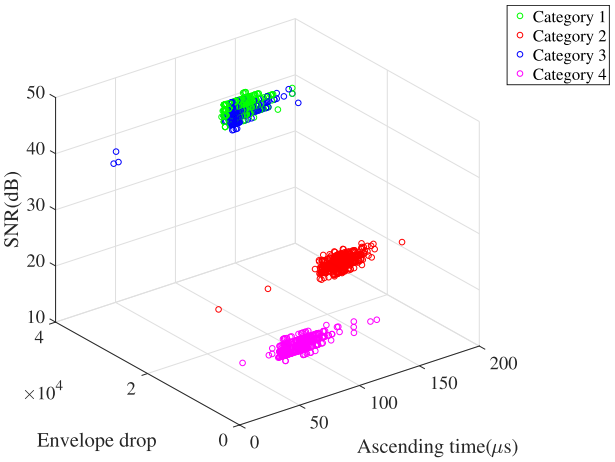

FIGURE 17. The identification result of feedback classification algorithm for environment 2.

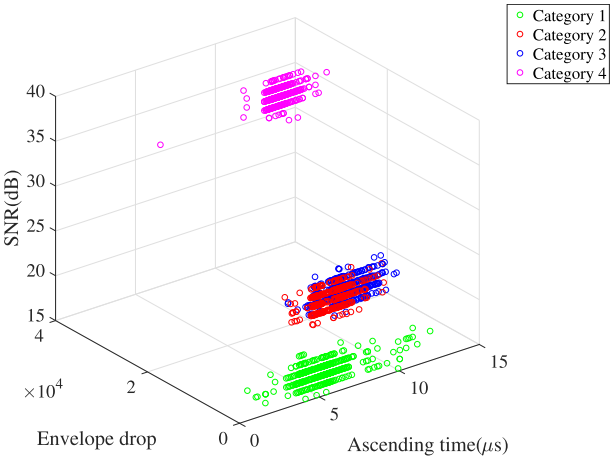

FIGURE 18. The identification result of feedback classification algorithm for environment 3.

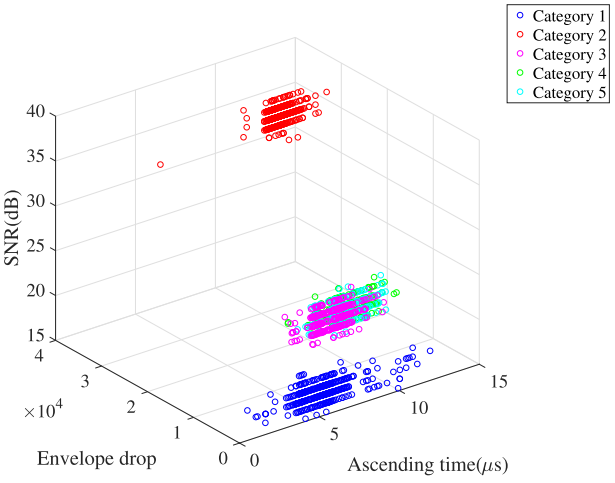

FIGURE 19. The identification result of the improved K-Means algorithm for environment 1($K = 5$).

with the proposed algorithm, but the accuracy rates are much lower than the feedback classification algorithm proposed in this paper.

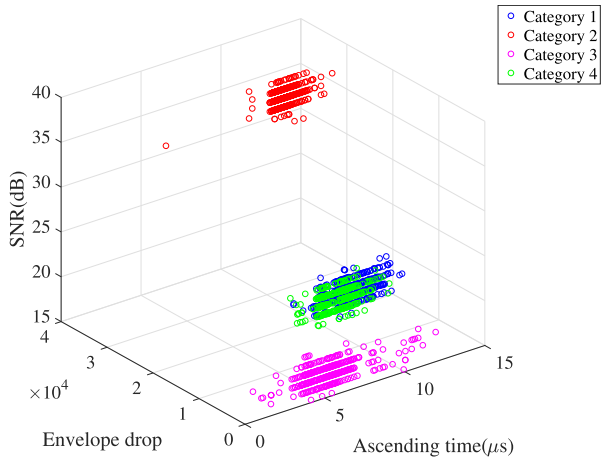

FIGURE 20. The identification result of the improved K-Means algorithm for environment 1($K = 4$).

TABLE 4. Identification performances of the improved K-Means algorithm ($K = 5$).

Identification Performances	Individual Source ID				
	1	2	3	4	5
Identification rate (%)	99.41	99.14	100.00	100.00	-
Accuracy rate (%)	100.00	98.05	99.22	45.03	54.00
Global accuracy rate (%)	85.87				

TABLE 5. Identification performances of the improved K-Means algorithm ($K = 4$).

Identification Performances	Individual Source ID			
	1	2	3	4
Identification rate (%)	98.07	99.01	100.00	100.00
Accuracy rate (%)	97.66	100.00	99.22	98.83
Global accuracy rate (%)	99.27			

By comparing the proposed feedback classification algorithm and the improved K-Means algorithm, it is found the identification performance of the improved K-Means algorithm is very poor when the value of K calculated by the improved K-Means algorithm is not correct. Even if K is correctly calculated, the identification and accuracy rates of the improved K-Means algorithm are still slightly lower than the feedback classification algorithm proposed in this paper. This is because there are some points whose distances away from the centers are almost the same in different categories.

Therefore, by fully exploiting the moving state of a specific emitter source, the number of specific emitter individuals can be further determined. Combined with the static and dynamic features of emitter individuals, the feedback classification algorithm proposed in this paper can accomplish the mobile SEI with more stable and effective performances.

VI. CONCLUSION

In this paper, we have proposed a method for mobile SEI when there is no prior knowledge. Novel moving state features and classification algorithm have been employed. Firstly, considering the differences in the inherent features and moving states of different emitter individuals, the Doppler frequency was adopted as dynamic features, and the envelope feature parameters and SNR was considered as static features to construct the signal fingerprint set. Secondly, the feedback classification algorithm composed of curve fitting and BP neural network was employed to accomplish the identification of signal fingerprints. Finally, simulation results in three different environments have shown that the proposed method can complete the identification of mobile specific emitter sources in the unsupervised state with high identification and accuracy rates.

REFERENCES

[1] P. Sui, Y. Guo, H. Li, S. Wang, and X. Yang, "Wavelet packet and granular computing with application to communication emitter recognition," *IEEE Access*, vol. 7, pp. 94717–94724, Jul. 2019.

[2] N.-X. Kang, M.-H. He, J. Han, and B.-Q. Wang, "Radar emitter fingerprint recognition based on bispectrum and SURF feature," in *Proc. CIE Int. Conf. Radar (RADAR)*, Guangzhou, China, Oct. 2016, pp. 1–5.

[3] J. Zhang, F. Wang, O. A. Dobre, and Z. Zhong, "Specific emitter identification via Hilbert–Huang transform in single-hop and relaying scenarios," *IEEE Trans. Inf. Forensics Security*, vol. 11, no. 6, pp. 1192–1205, Jun. 2016.

[4] Y. Yuan, Z. Huang, H. Wu, and X. Wang, "Specific emitter identification based on Hilbert–Huang transform-based time–frequency–energy distribution features," *IET Commun.*, vol. 8, no. 13, pp. 2404–2412, Sep. 2014.

[5] A. Kawalec and R. Owczarek, "Radar emitter recognition using intrapulse data," in *Proc. 15th Int. Conf. Microw., Radar Wireless Commun.*, Warsaw, Poland, Dec. 2004, pp. 435–438.

[6] J. Zhang, F. Wang, Z. Zhong, and O. Dobre, "Novel Hilbert spectrum-based specific emitter identification for single-hop and relaying scenarios," in *Proc. IEEE Global Commun. Conf. (GLOBECOM)*, San Diego, CA, USA, Dec. 2015, pp. 1–6.

[7] K. Sa, D. Lang, C. Wang, and Y. Bai, "Specific emitter identification techniques for the Internet of Things," *IEEE Access*, vol. 8, pp. 1644–1652, 2020.

[8] K. Liu, J. Wang, and X. Meng, "A new method for identifying radar emitter based on self-distilled pulse sequence pattern," *Electron. Opt. Control*, vol. 20, no. 12, pp. 73–76, Dec. 2013.

[9] C. Chen, M. He, and H. Li, "An improved radar emitter recognition method based on Dezert-Smarandache theory," *Chin. J. Electron.*, vol. 24, no. 3, pp. 611–615, Jul. 2015.

[10] J.-H. Liang, Z.-T. Huang, and Z.-W. Li, "Method of empirical mode decomposition in specific emitter identification," *Wireless Pers. Commun.*, vol. 96, no. 2, pp. 2447–2461, May 2017.

[11] K. Gençol, A. Kara, and N. At, "Improvements on deinterleaving of radar pulses in dynamically varying signal environments," *Digit. Signal Process.*, vol. 69, pp. 86–93, Oct. 2017.

[12] X. Xu, W. Wang, and J. Wang, "A three-way incremental-learning algorithm for radar emitter identification," *Frontiers Comput. Sci.*, vol. 10, no. 4, pp. 673–688, Aug. 2016.

[13] L. J. Wong, W. C. Headley, S. Andrews, R. M. Gerdes, and A. J. Michaels, "Clustering learned CNN features from raw I/Q data for emitter identification," in *Proc. MILCOM-IEEE Mil. Commun. Conf. (MILCOM)*, Los Angeles, CA, USA, Oct. 2018, pp. 26–33.

[14] Q. Zhao, Q. Zhang, and Y. Yuan, "An improved non-cooperative signal detection and extraction method based on template matching," in *Proc. 7th IEEE Int. Conf. Electron. Inf. Emergency Commun. (ICEIEC)*, Macau, China, Jul. 2017, pp. 365–368.

[15] M. Mohammadkarimi, E. Karami, O. A. Dobre, and M. Z. Win, "Doppler spread estimation in MIMO frequency-selective fading channels," *IEEE Trans. Wireless Commun.*, vol. 17, no. 3, pp. 1951–1965, Mar. 2018.

[16] S. M. Kay, *Fundamentals of Statistical Signal Processing: Estimation Theory*, vol. 1. Englewood Cliffs, NJ, USA: Prentice-Hall, 1993.

[17] C. Shang and J. Chen, "SNR estimation based on M2M4 algorithm for QPSK signal," *Radio Eng.*, vol. 48, no. 9, pp. 756–759, Sep. 2018.

[18] W. Wang and G. Hu, "Statistical performance analysis of the M2M4 based SNR estimator," *Mod. Radar*, vol. 34, no. 8, pp. 42–45, Aug. 2012.
[19] H. Wang, G. Zhao, and Y. Wang, "Specific emitter identification based on higher order moment of the envelope's front edge," *Mod. Radar*, vol. 32, no. 10, pp. 42–45, Oct. 2010.
[20] L. Jin, G. Huang, P. Li, and Y. Wei, "Technology of special emitter identification and verification based on envelope fingerprint features," *Mod. Radar*, vol. 42, no. 1, pp. 28–31, Jan. 2020.
[21] C. Luo and X. Liu, "Realization method to curve fitting based on MATLAB," *Mod. Electron.*, vol. 163, no. 20, pp. 16–17, Oct. 2003.
[22] W. Feng, J. Wang, and W. Tian, "Design and implementation of flight track simulation system," *Comput. Simul.*, vol. 27, no. 12, pp. 47–50, Dec. 2010.
[23] H. Jiang, L. Zeng, and J. Hu, "The design and performance of optimal BP neural network classifier," *Comput. Eng. Appl.*, vol. 37, no. 5, pp. 122–125, May 2001.
[24] H. Liu, Z. Liu, W. Jiang, and Y. Zhou, "Incremental learning approach based on vector neural network for emitter identification," *IET Signal Process.*, vol. 4, no. 1, pp. 45–54, Feb. 2010.
[25] Y. Zeng, Q. Wu, and R. Zhang, "Accessing from the sky: A tutorial on UAV communications for 5G and beyond," *Proc. IEEE*, vol. 107, no. 12, pp. 2327–2375, Dec. 2019.

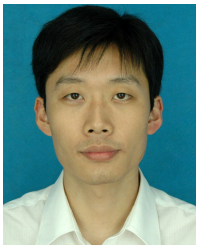

QIN ZHANG received the B.Eng. and Ph.D. degrees from the Beijing Institute of Technology, Beijing, in 2003 and 2008, respectively. He is currently a Lecturer with the Beijing Institute of Technology. His research interests include communication engineering, digital signal processing, and intelligent algorithms.

YU GUO received the B.Eng. degree in information and communication engineering from Beijing Jiaotong University, Beijing, China, in 2018. He is currently pursuing the M.Eng. degree in information and communication with the Beijing Institute of Technology, Beijing. His research interests include digital signal processing and specific emitter identification.

ZHENGYU SONG received the B.Sc. and M.Sc. degrees from Beijing Jiaotong University, Beijing, China, and the Ph.D. degree from the Beijing Institute of Technology, Beijing, all in information and communication engineering. He is currently with the School of Electronic and Information Engineering, Beijing Jiaotong University. His main research interests include radio resource management in non-orthogonal multiple access systems, the Internet of Things, mobile edge computing, and terrestrial-satellite integrated communications.